Microsystem Technologies (2020) 26:475–487
https://doi.org/10.1007/s00542-019-04536-7

TECHNICAL PAPER

Design, modeling and experimental evaluation of a legged, multi-vectored water-jet composite driving mechanism for an amphibious spherical robot

Huiming Xing[1] · Shuxiang Guo[1,2] · Liwei Shi[1] · Xihuan Hou[1] · Yu Liu[1] · Huikang Liu[1]

Received: 26 April 2019 / Accepted: 5 July 2019 / Published online: 25 July 2019

Abstract
This paper designs a novel legged, multi-vectored water-jet composite driving mechanism (LMWCDM) for the amphibious spherical robot (ASRobot) and presents modeling and experimental evaluation of this composite driving mechanism. In order to crawl on land flexibly, the robot was designed in SolidWorks and simulated in ADAMS environment with the sit to stand motion and a crawling gait. Then the simulation results, such as driving torques, guided the selection of servomotors in different joints. In aquatic environment, the dynamic modeling of ASRobot was analyzed by synthesizing the propulsive vectors of four propellers in each workspace of legs. Simplistically, multiple underwater locomotion, such as longitudinal and lateral motion, rotary motion, sinking and floating motion and cruising motion, were proposed. Thus, using a six-axis force/torque sensor at the equivalent mass center, a force and torque measuring mechanism was developed to obtain the direct propulsive effect and validate the modeling of the driving system. To evaluate the robot design and selection of servomotors, experiments of the sit to stand motion and crawling motion were conducted. Underwater testing experiments of LMWCDM were carried out to verify the modeling of rotary motion, sinking and floating motion. Besides, underwater test of the robot prototype also proved the highly flexible and swift motion.

1 Introduction

In recent years, much attention has been focused on the amphibious robot in the field of robotics. Owing to their terrestrial and aquatic ability, amphibious robots are widely used in a variety of high-risk tasks, such as monitoring and exploration in amphibious environment, pollution detection, submarine sampling, data collection, search and rescue after major natural disasters, and scientific investigation.

To achieve amphibious locomotion in complex environmental conditions, plenty of research have been conducted to propose and develop various interesting propulsive mechanisms or robotic platforms. Kim et al. (2016) developed an amphibious robot prototype. It used the buoyancy generated by spherical styrofoam to operate on water and adopted the Klann mechanism and a tripod gait to walk on the ground. The shortcoming of the robot is that it cannot operate in water. Zhang et al. (2016) developed the amphibious robot named AmphiHex-I which walked on rough terrain, maneuvered underwater, and used specially designed transformable flipper legs to traverse soft muddy or sandy substrates in littoral areas between

✉ Shuxiang Guo
guoshuxiang@bit.edu.cn; guo@eng.kagawa-u.ac.jp

✉ Liwei Shi
shiliwei@bit.edu.cn

Huiming Xing
xinghuiming@bit.edu.cn

Xihuan Hou
houxihuan@bit.edu.cn

Yu Liu
liuyu_0827@bit.edu.cn

Huikang Liu
liuhuikang@bit.edu.cn

[1] Key Laboratory of Convergence Medical Engineering System and Healthcare Technology, Ministry of Industry and Information Technology, School of Life Science, Beijing Institute of Technology, Beijing 100081, China

[2] Faculty of Engineering, Kagawa University, 2217-20 Hayashicho, Takamatsu, Kagawa 761-0396, Japan

land and water. Zhong et al. (2018) proposed a new version—AmphiHex-II with a novel variable stiffness legs which combines the flexible flipper with the rigid fan-shaped leg structure in one propulsion mechanism. The on-land and underwater locomotion performance of AmphiHex-II was improved. But due to the heavy body, the robot has weak flexibility and difficulties of attitude control. Shen et al. (2017, 2016) proposed an amphibious robot with an eccentric paddle mechanism based on the epicyclic gear mechanism (ePaddle-EGM), and the robot can perform various terrestrial and aquatic gaits, such as the rotational paddling gait and the oscillating paddling gait. The ePaddle-EGM is a novel mechanism for amphibious locomotion, but the driving mechanism is quite complex for an amphibious robot. And due to the complex actuating mechanism, the measured thrust deviate greatly from the predicted thrust. Organisms that have evolved over thousands of years have high efficiency and advantages in complex movement. Now many amphibious robotic designs (Kim et al. 2016; Yang et al. 2015) have been inspired by biology (Shi et al. 2013, 2015a, b). Crespi and Ijspeert (2008) developed an amphibious snake robot named AmphiBot II that crawled and swam using a central-pattern generator. Guo et al. (2018) proposed a novel serpentine gait for snake-like robot based on the geometry mechanics. Crespi et al. (2013) designed a bio-amphibious salamander robot (Salamandra robotica II) that both walked and swam; the robot has four legs and an active spine allowing anguilliform swimming in water and on-ground walking with various gaits, featuring body–limb coordination and bodily undulation. Due to the multi-joints of these snake robots, it is hard to waterproofing for the robots. Besides, the snake robot has weak pose stability, which is not good for complex tasks, such as object tracking. In 2012 and 2013, Yu et al. designed an amphibious biomimetic fish-like robot termed AmphiRobot-II (Yu et al. 2012) with a wheel–propeller–fin mechanism and a specialized swivel mechanism (Yu et al. 2013); specifically, the wheel–propeller–fin mechanism functions as a drive wheel for crawling on land and as a common screw propeller or pectoral fin in water. However, the wheel-propeller-fin mechanism improve the complexity of the robot to realize the multiple locomotion on land and in water.

In the design of an amphibious robot, one of the most challenge is the driving mechanism, especially for the legged robot. In our previous study (Lin et al. 2013; Gu and Guo 2017; Guo et al. 2018; Li et al. et al. 2015, 2017; Xing et al. 2019; Zheng et al. 2018), inspired by amphibious turtles, we designed an amphibious robot (Xing et al. 2018) which is able to swim in water and crawl on land. But the robot has a heavy body that does not benefit on-land locomotion and the thrust of one water-jet propeller is only 80 mN, which was hard to actuate the robot with 8.2 kg. To overcome these deficiencies, a novel legged, multi-vectored water-jet composite driving mechanism was designed our new amphibious spherical robot shown in Fig. 1. Each leg with three joints can improve the flexibility and the adaptation of different terrains. On land, the robot walks with four legs smoothly. In water, a novel long-duct water-jet thruster (Hou et al. 2019) was designed as one part of the leg. The robot can swim with multi-vectored water-jet propellers system. Besides the high velocity and the capabilities of reducing the number of propellers, this vectored propulsion system has other superiority, such as the stabilization of the attitude of the vehicle to perform manipulation tasks, the high flexibility and mobility, rotation with zero-radius, and the accurate position control. However, it is a huge challenge to achieve flexible motion control with the vectored propulsion system. Jia et al. (2016) proposed an amphibious spherical robot with two arms mounting screw propellers. In water, it can realize thrust vectoring using the rotation of the arms, which can enhance its mobility to a large extent. But using the two actuators, it is hard to accomplish high precise attitude control. Jin et al. (2015) designed a new underwater robotic platform with a tilting thruster mechanism for hovering motion, which can implement six-degree-of-freedom (DOF) motion with only four thrusters with a selective switching control in real time. With this underwater robotic platform, Bak et al. (2017) proposed a new positioning controller using a vector decomposition method. Owing to the distribution of four thrusters with only one rotational axis, the robot has high performance of the attitude control. But according to the configuration of four thrusters, the robot is weak in the long-distance cruising. In this paper, the proposed multi-vectored water-jet propellers system can deal with this shortcoming. Using vectored thrust generated by water-jet thrusters in flexible legs, our robot can realize multi-locomotion, such as longitude and lateral motion, rotary motion, sinking and floating motion.

The remainder of this paper is organized as follows: In Sect. 2, we described our amphibious spherical robot with a legged, multi-vectored water-jet composite driving mechanism. Using ADAMS software, the driving torques of different joints in the sit to stand motion and a crawling gait were obtained to choose the type of servomotors in Sect. 3. Section 4 presented the underwater modeling of LMWCDM in the horizontal and vertical plane, and proposed multi-underwater locomotion mode. A measuring mechanism was designed to evaluate underwater modelling of LMWCDM in Sect. 4. In Sect. 5, experiments were conducted to validate the robot design and the selection of servomotors and evaluate the modeling of LMWCDM in multi-underwater motion. The robot prototype was also

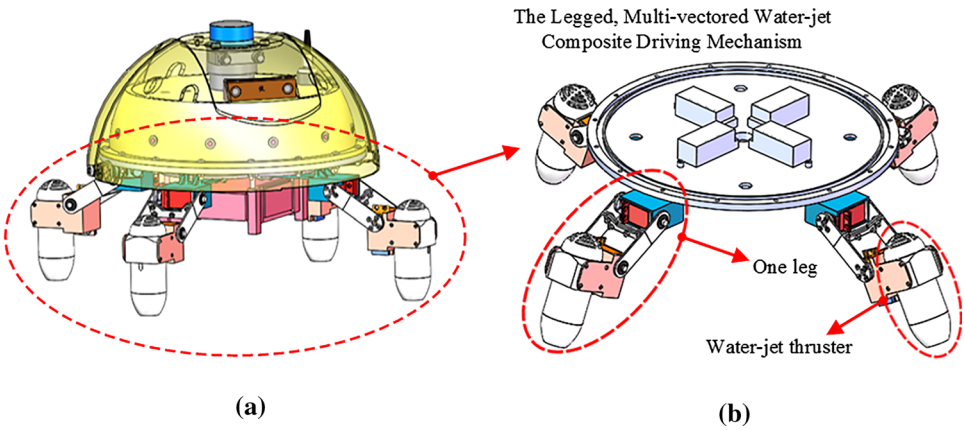

Fig. 1 **a** Developed the novel amphibious robot; **b** the legged, multi-vectored water-jet composite driving mechanism

tested in water. Section 6 concluded this paper and future work.

2 The legged, multi-vectored water-jet composite driving mechanism

For our amphibious robot, the on-land and underwater locomotion rely on the legged, multi-vectored water-jet composite driving mechanism (Xing et al. 2018). The robot walks on land or on the riverbed with the legged mode. In water, the robot swims via the vectored thrust generated by the multi-vectored water-jet thrusters. As depicted in Fig. 2a, the composite driving mechanism has the radially free distributed structure which is more superior than the traditional ones. The mechanism is composed of four mechanical legs and four cambered slides. As shown in Fig. 2b, the mechanical leg is composed of three digital servomotors, three connecting rod parts and one duct-type water-jet electric propeller. Three connecting rod parts are respectively defined as coxa, femur and tibia. The joints connecting these parts are named as follows: the joint connecting the body and coxa is thoraco-coxal joint (TC-joint), which enables the leg's forward and backward movements; the joint connecting the coxa and femur is the coxa-trochanteral joint (CTr-joint), which enables elevation and depression of the leg; the joint connecting the femur and tibia is the femur-tibia joint (FTi-joint), which enable extension and flexion of the tibia. All of these three joints are active joints actuated by servomotors named as Coxa Servomotor (CS), Femur Servomotor (FS) and Tibia Servomotor (TS).

On land, the driving mechanism can assist the robot in walking like a quadruped robot. Due to the heavy leg, the CS will have a big downward force while the leg is lifted. In order to make the leg move flexibly, the cambered slides are designed to prevent the downward force. The bearings make the legs rotate between the cambered slides and the middle plate. Due to the well waterproofing of our robot, our robot also can walk on the bed for exploring in underwater narrow caves. In water, with vectored thrust generated by four water-jet thrusters, the driving mechanism can generate vectored thrust to push the robot forward, backward, rotation, upward and downward. Compared with these existing vectored propulsion systems,

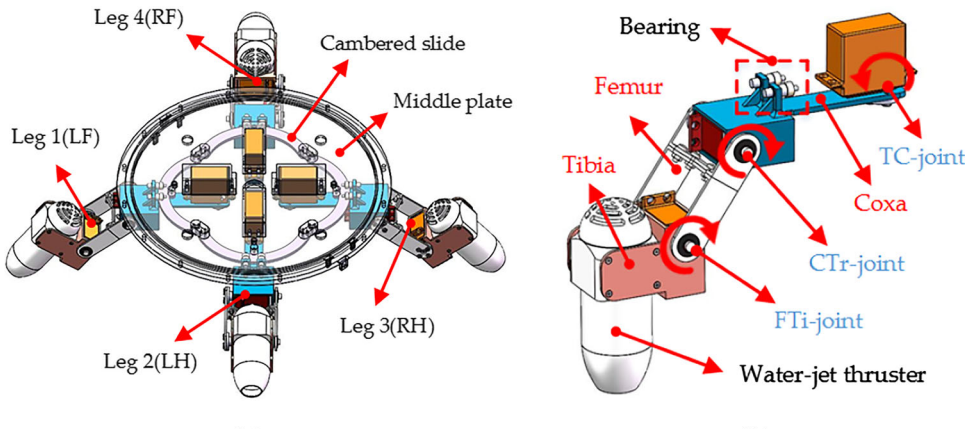

Fig. 2 **a** The composite driving mechanism; **b** the structure of one leg

this mechanism only has four thrusters. And with the configuration of legs, this mechanism has high efficiency.

The most key feature of the robot is that its legs can rotate around the output axis of the CS. The bearings were mounted on the link of its legs, which makes the leg move smoothly between the cambered slides and the middle plate. Thus, each leg has 5 degrees of freedom which enable it to move more flexibly on land. And in water, along with the adjustment of the angle of legs, the robot can realize the real-time multi-vectored control strategy, which makes the robot swim more swiftly.

3 Simulation in the ADAMS environment

To keep the robot move and rotate steadily and flexibly with its structural design, the choice of servomotors in different joints is essential. In this section, we built a virtual model of the prototype in the ADAMS environment. Here are two main methods to establish a virtual model of the prototype in ADAMS software. One is building the 3D model and conducting simulation in ADAMS directly. However, the ADAMS software did not specialise the design of the entity model, but is specially used for simulation. Therefore, the other method is to build the model firstly with SolidWorks, Pro/E or UG; Then import it into ADAMS software. As mentioned above, the model of our robot was designed by SolidWorks 2017. In order to import the model and simulate in the ADAMS, the format of the model was saved as a parasolid (*.xt file). After imported into ADAMS, the model of our robot loses parameters, such as weight and the materal of the component. Therefore, reseting these parameters, such as weight, motion function, constrain conditions and forces, are essential.

3.1 On-land gaits

For quadruped robots, the gaits can be divided into symmetrical and asymmetrical gaits (Li et al. 2015). The symmetrical gait is basically a two-beat gait, such as pacing, trotting and gallop. And the asymmetrical gait is basically a four-beat gait, such as crawling. Considering the two-beat gait which cause the unstable movement and the abrasion of the structure, the stable four-beat gait (crawling) was analyzed in this paper. To describe the locomotion of the legged robot simply, the four legs were termed LF, LH, RH, and RF (the left foreleg, left hind leg, right hind leg, and right foreleg, respectively; Fig. 2a). As shown in Fig. 3a, the sequence of the crawling gait in one cycle was "LH → LF → RH → RF". And each leg performs a series of cycles "lift-swing-fall-support." The gray bar indicates the transfer phase, and the black and blue bars show the support phase. Over single cycle of the crawling gait, the robot moves the body twice in support phase (blue bar) with four legs. Compared with the previous robot, ASRobot with three joints has advantages in flexibility, maneuverability and adaptability. In order to describe the gait clearly, the diagram of the gait was shown in Fig. 3b. We can see that there are always three or more legs supporting the body. In the situation of three legs supporting the body, the connection of footholds forms a acute triangle, which can keep the body steadily.

3.2 Simulation of driving torqure in different joints

By applying several related constraints and driving force to the virtual prototype model, its actual crawling gait was simulated in ADAMS. As shown in Fig. 4, the robot completed the sit to stand motion (Fig. 4a, b) and the crawling motion (Fig. 4c–h). The simulation animation results could be viewed in the post-processing module of ADAMS. The simulation aims to choose a appropriate servomotors. Therefore, the displacement curves of the centroid and the driving torque of each joint were obtained during the simulation process.

As shown in Fig. 5, the robot conducted the sit to stand motion between 0 and 1 s. we concluded that the driving torque of TC-joint is quite small, and the driving torques of CTr-joint and FTi-joint are up to 2200 N mm and 1300 N mm.

The crawling torque curves of different joints in LF was depicted from 1 to 25 s (Fig. 5), and we can draw the following conclusions. First, the driving torques of CTr-

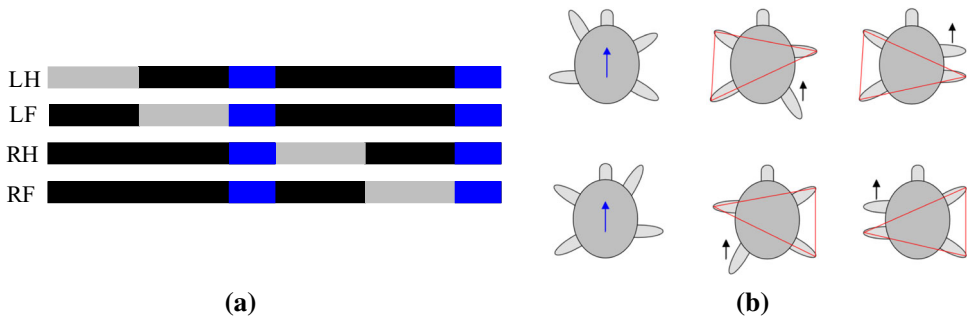

Fig. 3 **a** The sequence of the crawling gait; **b** the diagram of the crawling gait. The gray indicates the transfer phase, and the black and blue bars show that the leg is in the support phase which includes the body moving phase

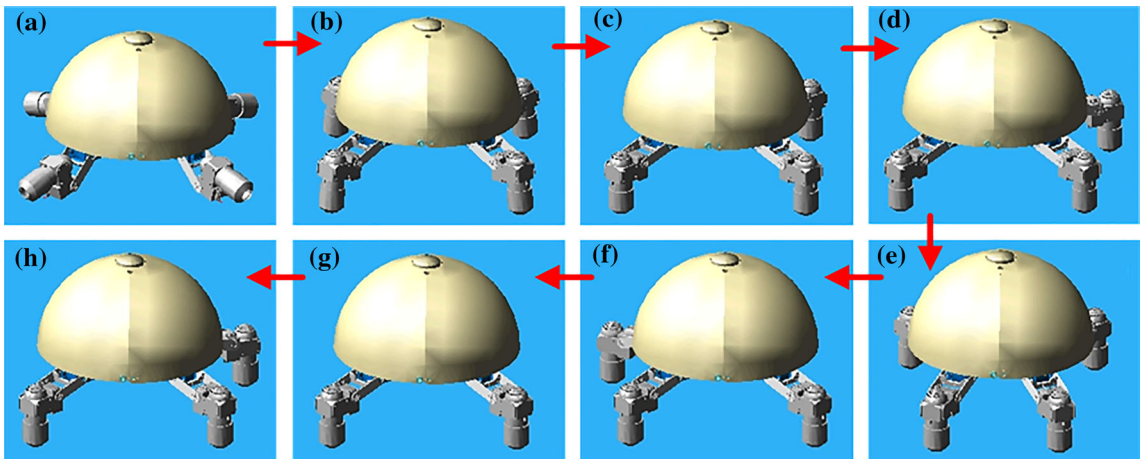

Fig. 4 The model in the ADAMS environment. **a**, **b** The sit to stand motion; **c**–**h** the crawling motion

joint and FTi are greater than that of the TC-joint; this is due to support the heavy body of ASRobot while crawling, and the TC-joint only swing the mechanical leg. The curves of driving torque appear abrupt and form spikes, which will induce unbalanced moment and impact the stability of ASRobot. Secondly, for CTr-joint and FTi-joint, the driving torque of the support phase is much larger than the transfer phase. This is because four legs support the body in the support phase and three legs support in the transfer phase. Thirdly, the maximum driving torque of TC-joint basically remained steady, below 750 N mm, when the TC-joint was in the supporting phase, and the maximum driving torque of CTr-joint and FTi-joint remained steady, below 2250 N mm and 1000 N mm, respectively. Based on the simulation results of driving torques, the driving torques of TC-joint, CTr-joint and FTi-joint need to be more than 800 N mm, 2250 N mm and 1300 N mm, respectively. Considering the sensors added in the future, the selected servomotors was shown in Table 1.

4 Underwater dynamic modeling of LMWCDM

4.1 Mechanics of LMWCDM

As shown in Fig. 6a, with four 90° symmetrical vector disposition of the horizontal and vertical propellers, the ASRobot has 6 DoFs and robust underwater motion under side disturbances. We analyze the propulsion system in two cases: the horizontal propulsion and vertical propulsion.

In horizontal plane, each leg is rotated by the servo-motor (CS), so it can rotate around its axis within the bound $\theta_1^i \in [0, \pi/2]$ (rad), $i = 1, 2, 3, 4$. The force F_X, F_Y and T_Z can be determined by the horizontal force F_H^i $(i = 1, 2, 3, 4)$.

The propulsive force along the X axis and Y axis:

$$\begin{cases} F_X = F_X^1 - F_X^2 - F_X^3 + F_X^4 \\ F_Y = -F_Y^1 - F_Y^2 + F_Y^3 + F_Y^4 \end{cases} \tag{1}$$

where, $F_X^i = F_H^i \sin\theta_1^i \quad (i = 1, 2, 3, 4), \quad F_Y^i = F_H^i \cos\theta_1^i$ $(i = 1, 2, 3, 4)$.

The moment on the Z axis:

$$\begin{aligned} T_Z = al\big[&F_H^1(c_1^1 - s_1^1) + F_H^3(c_1^3 - s_1^3) \\ &- F_H^2(c_1^2 - s_1^2) - F_H^4(c_1^4 - s_1^4)\big] \end{aligned} \tag{2}$$

where, l is the distance from the axis of CS to the center.

In the vertical plane, as shown in Fig. 6b, the vertical thrust F_V^i $(i = 1, 2, 3, 4)$ generated by the propeller can produce the force F_Z and the torque T_X and T_Y.

The total vertical force on the Z axis:

$$F_Z = \sum_{i=1}^{4} F_V^i = \sum_{i=1}^{4} F^i s_{23}^i \tag{3}$$

The moment on the X axis and Y axis:

$$\begin{cases} T_X = al(-F_V^1 - F_V^2 + F_V^3 + F_V^4) \\ T_Y = al(-F_V^1 + F_V^2 + F_V^3 - F_V^4) \end{cases} \tag{4}$$

Therefore, the force matrix $\mathbf{F}_B = [F_X \quad F_Y \quad F_Z]^T$ can be obtained by Eq. (5).

$$\mathbf{F}_B = \mathbf{M}_F \mathbf{F}_P \tag{5}$$

where, the force vector of propellers $\mathbf{F}_B = [F^1 \quad F^2 \quad F^3 \quad F^4]^T$, $s_1 = \sin\theta_1$, $c_1 = \cos\theta_1$, $s_{23} = \sin(\theta_2 + \theta_3)$ and $c_{23} = \cos(\theta_2 + \theta_3)$ and

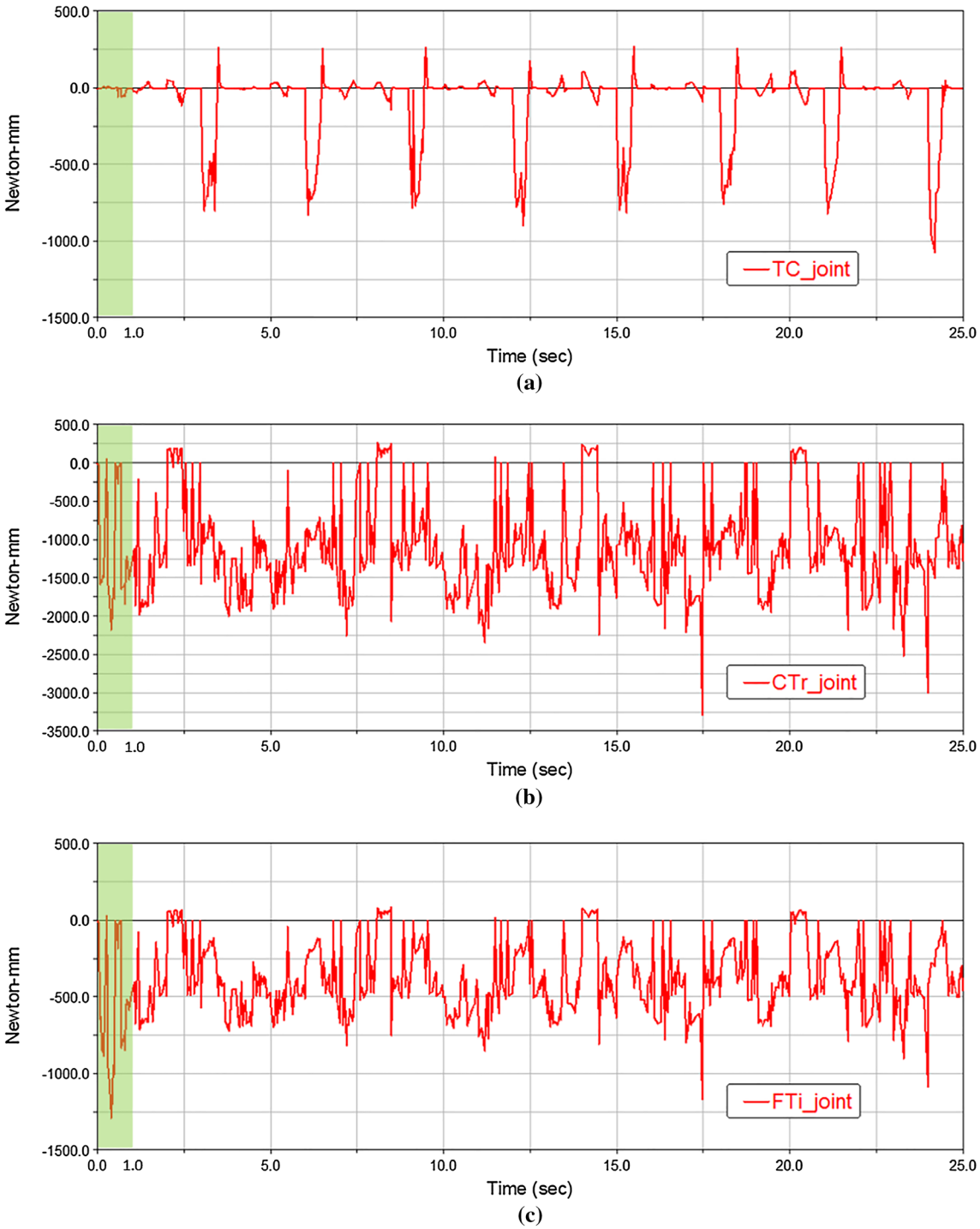

Fig. 5 The torque of three joints in LF in sit to stand motion and crawling motion. **a** The torque of TC-joint; **b** the torque of CTr-joint; **c** the torque of FTi-joint

$$\mathbf{M}_F = \begin{bmatrix} s_1^1 c_{23}^1 & -s_1^2 c_{23}^2 & -s_1^3 c_{23}^3 & s_1^4 c_{23}^4 \\ -c_1^1 c_{23}^1 & -c_1^2 c_{23}^2 & c_1^3 c_{23}^3 & c_1^4 c_{23}^4 \\ s_{23}^1 & s_{23}^2 & s_{23}^3 & s_{23}^4 \end{bmatrix} \tag{6}$$

And, the moment matrix $\mathbf{T}_B = [\,T_X \quad T_Y \quad T_Z\,]^T$ can be obtained by Eq. (7).

$$\mathbf{T}_B = al\mathbf{M}_T\mathbf{F}_P \tag{7}$$

where, $a = \sqrt{2}/2$, and

$$\mathbf{M}_T = \begin{bmatrix} -s_{23}^1 & -s_{23}^2 & s_{23}^3 & s_{23}^4 \\ -s_{23}^1 & s_{23}^2 & s_{23}^3 & -s_{23}^4 \\ (c_1^1 - s_1^1)c_{23}^1 & -(c_1^2 - s_1^2)c_{23}^2 & (c_1^3 - s_1^3)c_{23}^3 & -(c_1^4 - s_1^4)c_{23}^4 \end{bmatrix}$$

Table 1 Specification of servomotors in different joints

Servo motors	
CS	6.6 V, 23 kg cm, 0.12 s/60°
FS	8.4 V, 38 kg cm, 0.12 s/60°
TS	6.6 V, 23 kg cm, 0.12 s/60°

4.2 Underwater locomotion modes

In our robot, each water-jet thruster of four legs with three servomotors can rotate in the vertical and horizontal planes. In order to describe the model of the leg simply, three coordinate systems $\{O_1^1 - X_1^1Y_1^1Z_1^1$, $O_2^1 - X_2^1Y_2^1Z_2^1$ and $O_3^1 - X_3^1Y_3^1Z_3^1\}$ shown in Fig. 7a are defined in the TC-joint, CTr-joint and FTi-joint of LF, respectively. Due to the limitation of the mechanical structure, the angles θ_1^1, θ_2^1 and θ_3^1 that rotate around the z axis of $O_1^1 - X_1^1Y_1^1Z_1^1$, the y axis of $O_2^1 - X_2^1Y_2^1Z_2^1$ and the Z axis of $O_3^1 - X_3^1Y_3^1Z_3^1$ have a limited range, i.e., $\theta_1^1 \in [0 \quad \pi/2]$, $\theta_2^1 \in [-\pi/2 \quad \pi/6]$ and $\theta_3^1 \in [-\pi/2 \quad \pi/3]$. In order to draw the whole workspace of LF, we chose the coordinate of TC-joint as the base coordinate $(0, 0, 0)$, and the angle θ_3^1 is set to be 19.5°. As shown in Fig. 7b, varying with the angle θ_1^1 and θ_2^1, the position of the nozzle generated a surface, and the position of the nozzle can be described by Eq. (8).

$$\begin{cases} x = [r_1 + (r_2 + r_3)\sin(\theta_1^1 + \pi/2)]\cos\theta_2^1 \\ y = [r_1 + (r_2 + r_3)\sin(\theta_1^1 + \pi/2)]\sin\theta_2^1 \\ z = -(r_2 + r_3)\cos(\theta_1^1 + \pi/2) \end{cases} \tag{8}$$

where, r_1, r_2 and r_3 are the length of the links.

The multi-locomotion is based on the workspace of each leg. In this paper, we analyzed underwater locomotion in the horizontal and vertical plane. As shown in Fig. 8a, b, with this configuration of legs ($\theta_1^1 = \theta_1^2 = \theta_1^3 = \theta_1^4 = \pi/2$, $\theta_2^1 = \theta_2^2 = \theta_2^3 = \theta_2^4 = 0$ and $\theta_3^1 = \theta_3^2 = \theta_3^3 = \theta_3^4 = 0$), the robot can realize longitudinal locomotion, i.e., forward motion and backward motion. The force F_X can be obtained by Eq. (1). In forward and backward motion, the

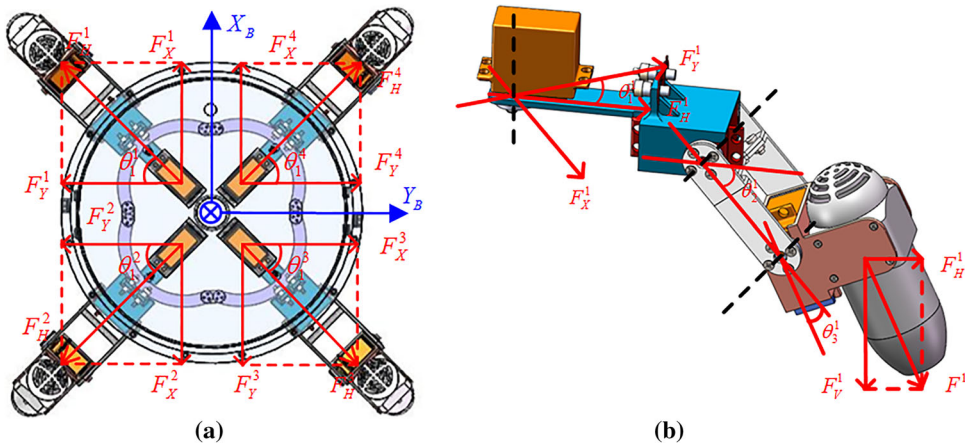

Fig. 6 **a** The force analysis of the propulsion system; **b** the force analysis of one leg

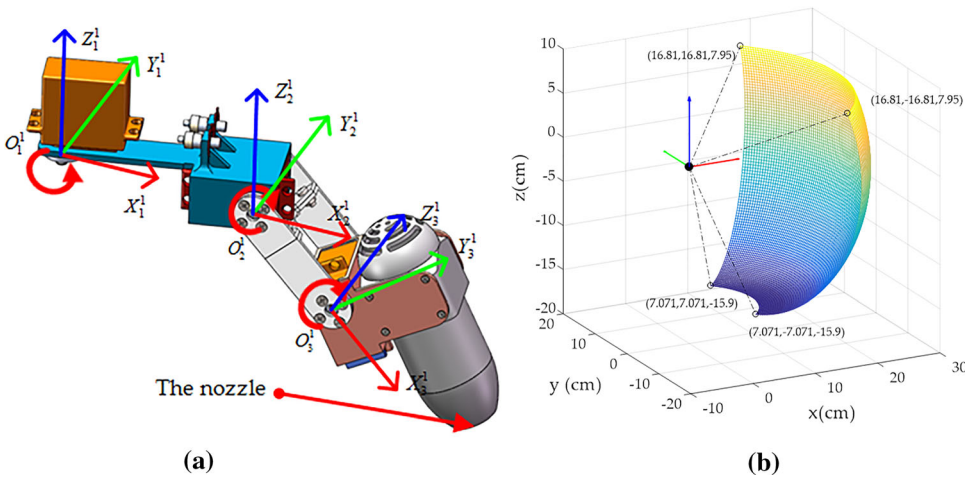

Fig. 7 **a** The coordinates of different joints in LF; **b** the workspace of LF

conditions are $F^1 = F^4 = 0$ and $F^2 = F^3 = 0$, respectively.

As shown in Fig. 8c, d, with this configuration of legs ($\theta_1^1 = \theta_1^2 = \theta_1^3 = \theta_1^4 = 0$, $\theta_2^1 = \theta_2^2 = \theta_2^3 = \theta_2^4 = 0$ and $\theta_3^1 = \theta_3^2 = \theta_3^3 = \theta_3^4 = 0$), the robot can realize lateral locomotion, i.e., rightward motion and leftward motion. The force F_Y can be obtained by Eq. (1). In rightward and leftward motion, the conditions are $F^1 = F^2 = 0$ and $F^3 = F^4 = 0$, respectively.

In the horizontal plane, the robot also can rotate with zero-radius. As shown in Fig. 8e, f, the varying angle θ_1^i of TC-joint will change the torque T_Z in this condition ($\theta_2^i + \theta_3^i = 0$, $i = 1, 2, 3, 4$). The torque can be calculated by

$$T_Z = al\left[F^1(c_1^1 - s_1^1) + F^3(c_1^3 - s_1^3) - F^2(c_1^2 - s_1^2) - F^4(c_1^4 - s_1^4)\right] \quad (9)$$

Besides the longitudinal and lateral locomotion, we analyzed underwater locomotion in the vertical plane, such as sinking and floating motion in submarine environment. As shown in Fig. 8g, h, with this configuration of legs ($\theta_1^1 = \theta_1^2 = \theta_1^3 = \theta_1^4 = \pi/4$), the robot can realize sinking and floating motion by changing the angles of CTr-joint and FTi-joint or the thrust of four propellers. The force F_Z can be obtained by

$$F_Z = \sum_{i=1}^{4} s_{23}^i F^i \quad (10)$$

If the robot needs to track the moving target or execute the task at different and remote place, the robot needs to possess the ability to cruise which can realize long-distance and high-speed underwater locomotion. As shown in Fig. 9a, b, four legs are rearranged to cruise in water. In the cruising underwater locomotion, the robot needs to turn right and left, sink and float. As depicted in Fig. 9, the robot can adjust the water-jet direction of thrusters in the vertical plane to realize sinking and floating motion while swimming forward. In addition, by the difference of the left water-jet force and the right water-jet force, the robot can implement the left and right turn motion. With the flexible motion, our robot can be used for environment monitoring, object tracking and detection of pollution with proper sensors.

4.3 The measuring mechanism for LMWCDM

For building the signals and the thrust of the single propeller, a six-axis force/torque sensor is utilized to sensing the force and torque. As shown in Fig. 10, this sensor consists of a transducer connector, Mounting Adapter Plate (MAP) and Tool Adapter Plate (TAP). And the coordinate system of the sensor is defined for describing the propulsive force. Figure 11 describes the measuring mechanism. The transducer connector is used to connect to the computer and transfer force and torque data. The MAP was mounted to the unmovable structure via U holders and connecters, and the TAP was used to fix to the water-jet propeller by a circular base plate, a circular disk and a

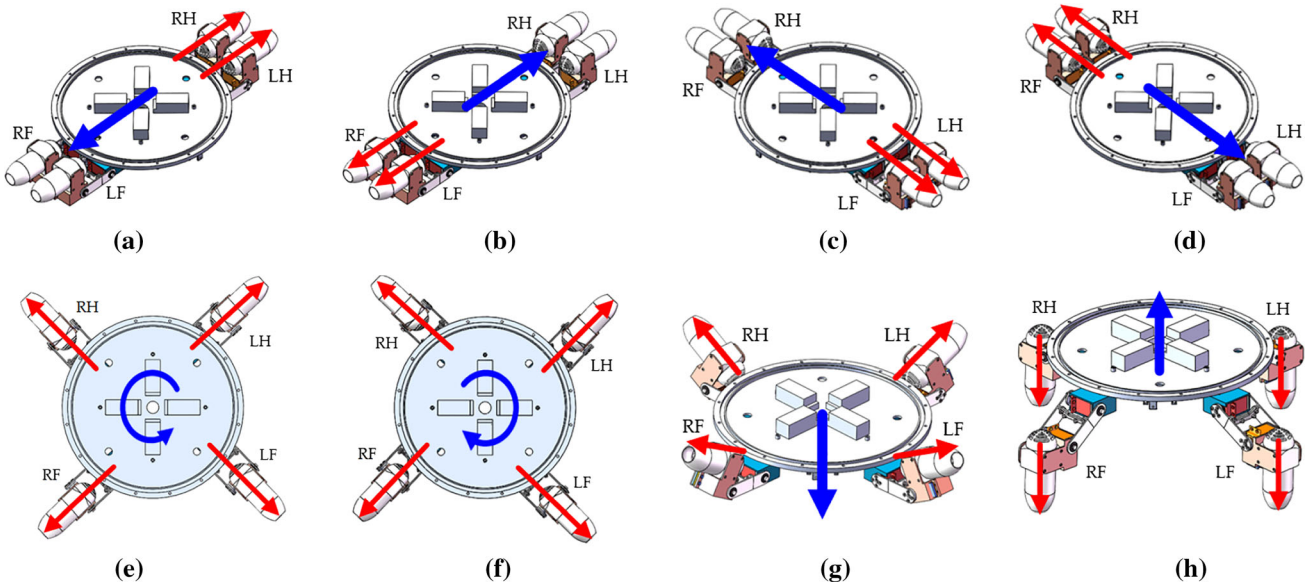

Fig. 8 Locomotion in horizontal and vertical plane. The blue arrow indicates the movement direction; the red arrow implies the water-jet direction of the propeller. **a** Forward motion; **b** backward motion; **c** rightward motion; **d** leftward motion; **e** right rotary motion; **f** left rotary motion; **g** sinking motion; **h** floating motion (color figure online)

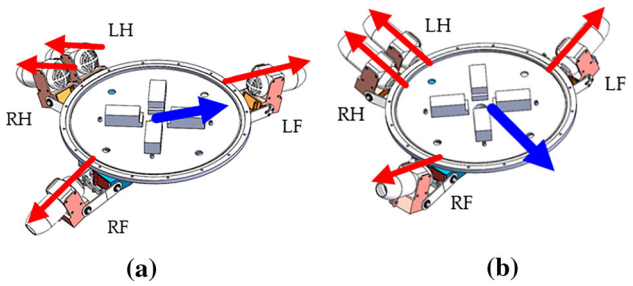

Fig. 9 The underwater cruising locomotion. **a** Cruising locomotion with floating; **b** cruising locomotion with sinking. The blue arrow indicates the motion direction; and the red arrow implies the water-jet direction (color figure online)

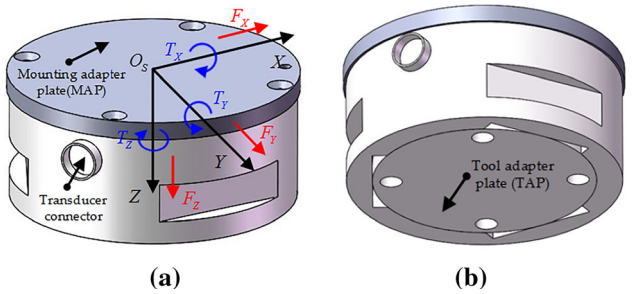

Fig. 10 The 3D model and its coordinate of the six-axis force/torque sensor. **a** Top view; **b** bottom view

connecter. In order to test the propulsive effect of one water-jet propeller, the mechanism need to be sink into the water. Therefore, a waterproof cylinder was used.

In terms of the motor control, the propulsive force f is changed by adjusting the PWM signals s. The frequency of PWM signal was set to 100 Hz. The relationship between the propulsive force and the PWM values can be obtained by the experimental method.

For every robot, in order to get the control of the position and posture more precisely and flexibly, the propulsive effect of the propulsion system needs to be informed in advance. Therefore, as shown in Fig. 12, the measuring mechanism was designed to measure all six components of the force and torque of LMWCDM. With different configurations of legs and different thrusts of propellers, the force and torque can be measured. And it will validate the underwater modelling of LWMCDM in Sect. 4.1. In the underwater locomotion, the measured force and torque will benefit the robot control in water.

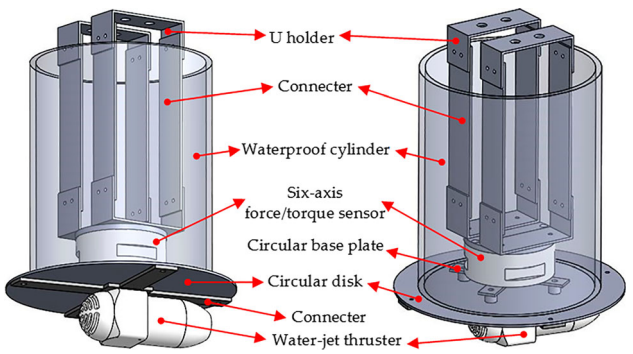

Fig. 11 The measuring mechanism of one water-jet thruster

5 LMWCDM verification experiments

For a driving mechanism of amphibious robot, LMWCDM needs to assist the robot in walking on land and swimming in water. In order to validate the design of LMWCDM and selection of servomotors, on land experiment was conducted firstly. Using the measuring mechanism, underwater testing experiments also were carried out to verify the underwater modeling of the typical locomotion modes, i.e., left and right rotary motion, sinking and floating motion. These experimental results will benefit the underwater motion of the robot.

5.1 On-land verification experiment of LMWCDM

In order to keep the balance of the gravity and buoyancy in water, the weight of the robot is up to 6.6 kg. Therefore, on-land locomotion is a dramatic challenge to our robot. In order to evaluate the robot design and the selection of our robot, experiments of the sit to stand motion, crawling and stand to sit motion are conducted. As shown in Fig. 13a, the robot is put on the ground of our laboratory with the sitting pose. Then, as shown in Figs. 13a–c, d–g, the robot stands up and crawls. After ten cycles of the crawling gait, as shown in Fig. 13h–j, the robot sits down. In these motions, the robot walks smoothly and flexibly. However, for lack of the force and torque measuring sensors in our robot, the force and torque of different joints is unable to be obtained. Therefore, the maximum load testing experiment is conducted to evaluate the ultimate capacity. When the extra load is above 1.1 kg, the unsteady motion appears. From the experimental results, the driving mechanism and the selection of servomotors is verified.

5.2 Calibration experiments of the water-jet thruster

For the purpose of obtaining the relationship between the propulsive force and the Pulse Width Modulation (PWM) signal, we need to find that how the propulsive force of the novel electric water-jet long-ducted propeller varies with the PWM values. Besides, allow for the difference of the propellers, the calibration of the water-jet thruster can generate the equal thrust with different control signals, which is essential for the robot.

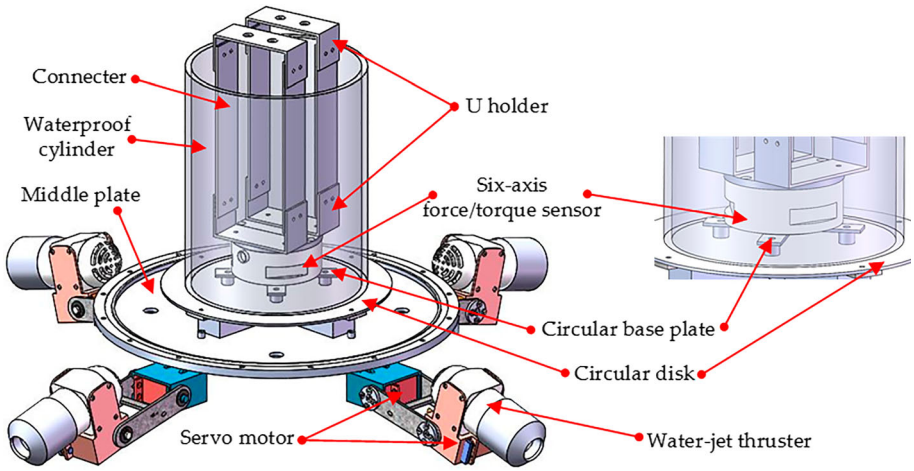

Fig. 12 The measuring mechanism of multi-vectored water-jet propulsion system

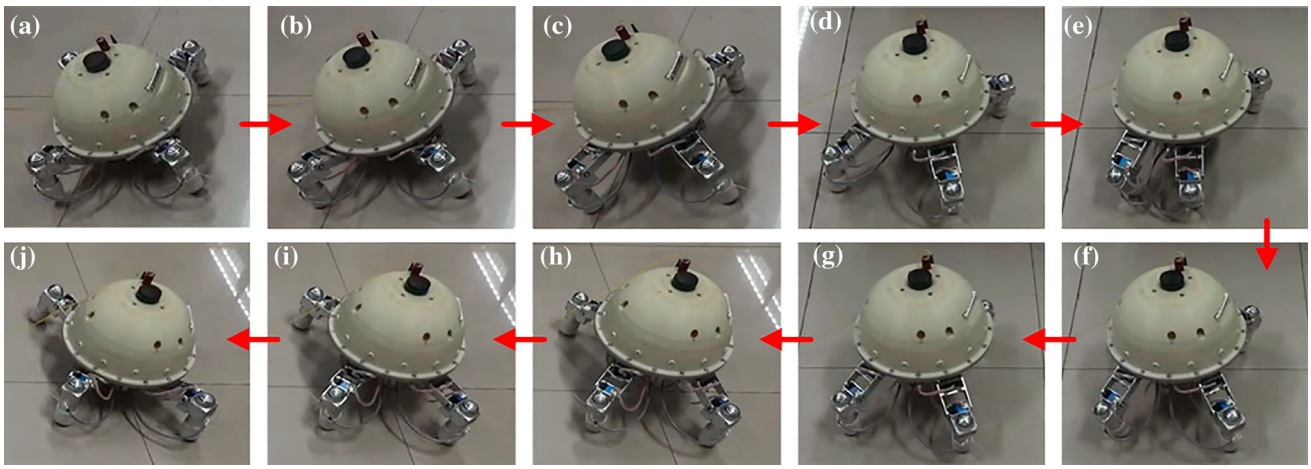

Fig. 13 Video snapshots of on-land experiment. **a–c** Sit to stand motion; **d–g** crawling motion; **h–j** stand to sit motion

The propeller is driven by a Brushless Electronic Speed Controller (ESC). Using the duty factor of the input PWM signal to ESC, the propeller's thrust can be controlled in an open loop. Then the experiments were conducted in the indoor pool with the size of 3 m × 2 m × 1 m (height × width × depth) without water flow disturbances. As shown in Fig. 14, the measuring mechanism was put into the water and the distance between the propeller and the water surface is 25 cm. With this depth, there is no water ejecting out of the water surface, which will keep the accuracy of the force measurement.

In the experiment, a bench top power (range 0–16 V, 0–3 A) was used for ESC. The frequency of the pulse width modulation (PWM) signal was 100 Hz, and the valid duty factor s ranged from 10 to 20%. As shown in Fig. 15, the star markers present the measured results of the force. These slight fluctuation data may be caused by the vibration of the experimental device. The red solid curve was the fitting curve of the blue star makers which is approximately linear, and the linear range was acquired from 12.4 to 19.2%. The small red points indicate the lower bound and upper bound. The thrust f of the propeller increased slightly while the duty factor is over 19.2%. The maximum thrust was 2.34 N with the 19.2% of PWM, about 30 times larger than the thrust (80 mN) of the thruster in our previous robot. Finally, the relationship between the PWM

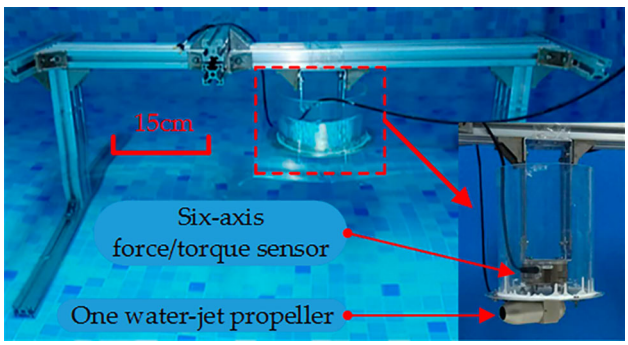

Fig. 14 The experimental setup of one water-jet propeller

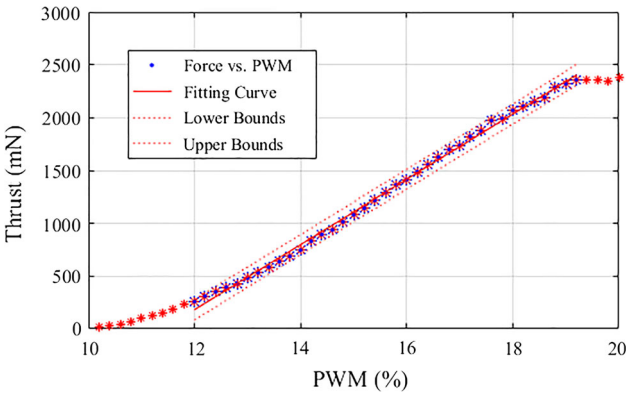

Fig. 15 The average propulsive force varying with PWM signals

signal and the thrust can be obtained and described by Eq. (11).

$$f = g(s) = 312.5s - 3586 \tag{11}$$

5.3 Underwater verification experiments of LMWCDM

For the purpose of guiding the control of the robot in real circumstance, two batteries with 8.4 V were employed in the experiment. As shown in Fig. 16, the propulsion system was mounted under the force/torque sensor using a rigid connector. To avoid the influence of the depth of water, we put the LMWCDM at the depth of 25 cm. Therefore, we designed the waterproof cylinder to protect the sensor. Avoiding the influence of the deformation, all the parts of this mechanism are rigid bodies. The LMWCDM was driven by the control board which generates 16 channels PWM. Four is for the propellers and twelve is to the servomotors. In order to evaluate the performance of the novel propulsion system and verify the underwater modeling of LMWCDM, we conducted experiments with rotary motion, sinking and floating motion.

In the left and right rotary motion, we set the PWM signal to the four water-jet thrusters as 14%, the angles θ_2^i and θ_3^i as 0°. And the angle θ_1^i varied from 0 to 90°. As shown in Fig. 16, the blue star makers indicate experimental results of the torque around z axis. The red curve is the simulated torque by Eq. (11). The maximum error and average error are up to 4.89 N mm and 2.65 N mm, which may be caused the shock of LMWCDM and the water flow. The black curve of the fitting torque is almost linear and high consistent with the simulated torque. The maximum torque can reach to be 80 N mm and the torque with the angle θ_2^i (45°) is almost zero. Due to the spherical shape of our robot, the viscous resistance is quiet slight and the torque is enough to rotate to the left or right smoothly.

The sinking and floating motion can be controlled by changing the angle θ_3^i and the thrust f of four propellers. Therefore, two experiments were conducted. In the first experiment, the angles θ_1^i and θ_2^i was set to be 45° and 0°, respectively. And the PWM signal of the thruster was set as 14% (750 mN). As shown in Fig. 17a, the thrust varies with the angle θ_1^i and the red curve is the simulated results by Eq. (11). Compared with the simulation forces, the maximum and average error are up to 200 mN and 86 mN. The black curve indicates the experimental forces on Z axis, and it achieved a high level of compliance with the simulated force, which verified the underwater modeling of the vertical locomotion.

In the second experiment, we set the angle θ_3^i as − 90°. As shown in Fig. 17b, the thrust along Z axis varied with the PWM signals (10.5–18%) to four thrusters. The thrust is almost linear from 12 to 15% and the decrease between 15 and 18% may be caused by the weak power supply. Therefore, the PWM signals from 12 to 15% was adapted to control the robot (Fig. 18).

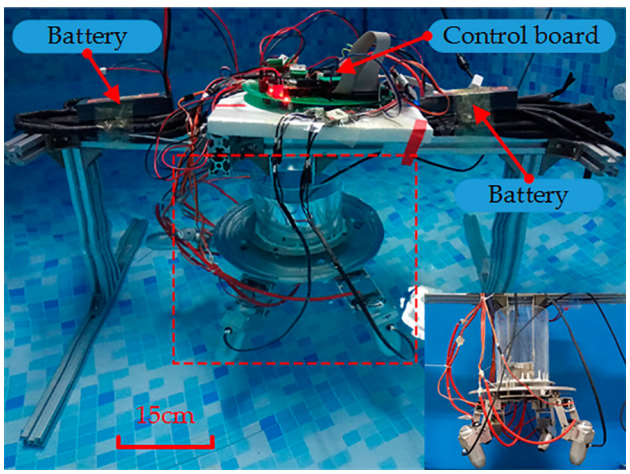

Fig. 16 The experimental setup of the propulsion system

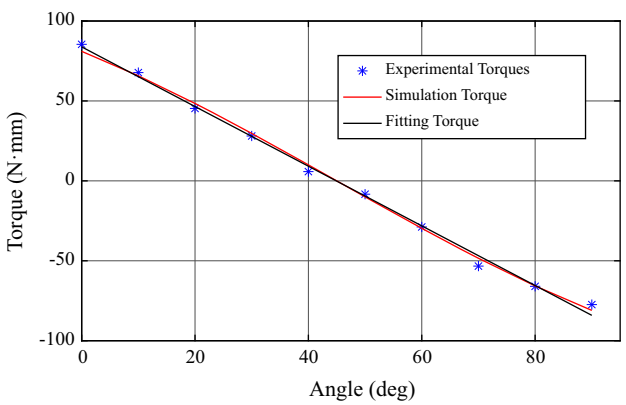

Fig. 17 Torque varying with angle θ_1^i

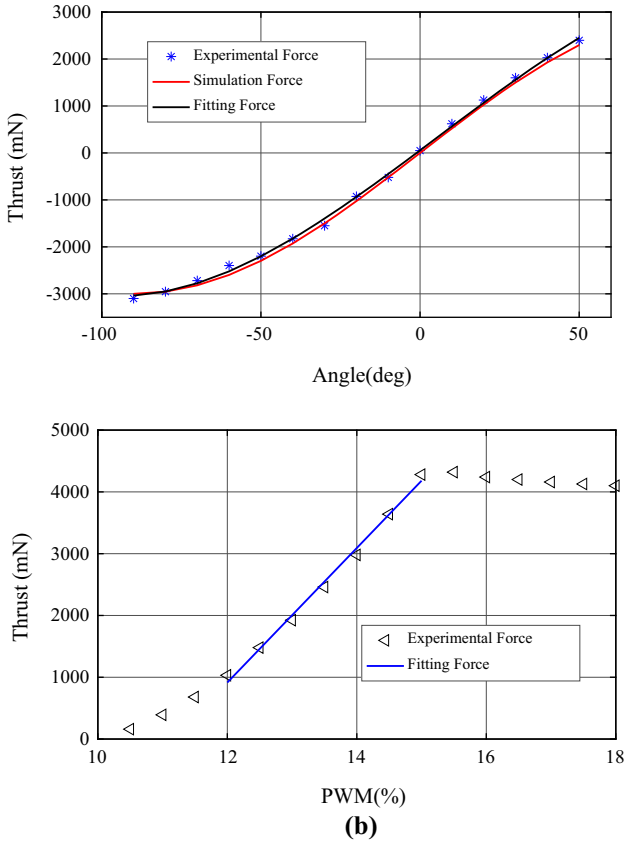

Fig. 18 Experimental data. **a** Thrust varying with angle θ_3^i; **b** thrust varying with PWM signals

5.4 Underwater test of the robot prototype

As shown in Fig. 19, the robot prototype was built for underwater locomotion. This underwater test was carried out in our lab pool, the size of which is 3 m × 2 m × 1 m (length × width × height). The robot was connected to a remote computer via an optical fiber cable. Therefore, the robot is able to be controlled by the computer. The robot can swim flexibly and swiftly, switch between different configuration mode smoothly. As shown in Fig. 19a, the robot can move forward and backward. As shown in Fig. 19b, the robot can sink down and float up. In underwater test, the robot can work about 110 min with this battery. The prolonged operation of the robot proved the good waterproofing.

6 Conclusions

This paper described design, modeling and experimental evaluation of a legged, multi-vectored water-jet composite driving mechanism (LMWCDM) for an amphibious spherical robot. The mechanism includes the legged mechanism and multi-vectored water-jet propulsion mechanism. Using Solidworks software, we designed the robot (6.6 kg). In order to select the type of the driving servomotors, the ADAMS simulation was used to draw the driving torque of different joints in legs with the crawling gait. By analyzing the simulation results, CTr-joint needs the largest driving torque, about 22.5 kg cm. The driving torque of TC-joint and FTi-joint are below 10 kg cm. Considering the expandability, servomotors with larger torques in different joints was selected. Besides, in submarine environment, the underwater dynamic modeling (forces and torques) of ASRobot can be obtained by synthesizing the propulsive vectors of four propellers. We also put forward multi-underwater locomotion via thruster vectoring, such as the longitude and lateral motion, the rotary motion, the vertical motion, and the cruising motion. Using a six-axis force/torque sensor at the equivalent mass center, a novel experimental mechanism was developed to evaluate the LMWCDM with different locomotion. Experiments of each thruster were conducted to establish the relationship between the pulse width module (PWM) signal and the thrust. And the linear range from 12.4 to 19.2% was acquired, the maximum thrust was 2.34 N with the 19.2% of PWM, about 30 times larger than the thrust (80 mN) of the previous robot. Then, further experiments with the vectored propulsion system were carried out, and these experimental results were in good agreement with the

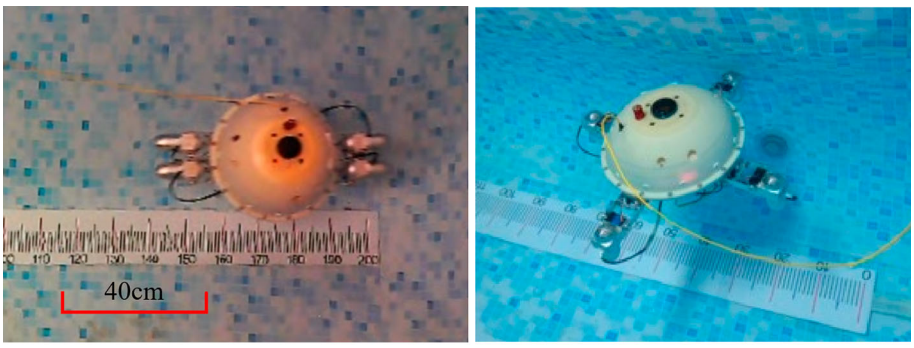

Fig. 19 The robot prototype in water. **a** Forward and backward mode; **b** floating and sinking mode

simulated results, which verified the underwater modeling of LMWCDM.

This process that confirm the type of motors in legs using ADAMS simulation, and the method to measure the force and torque of the propulsion system can guide to design other robots. In the future, we will focus on on-land locomotion and underwater locomotion of ASRobot.

Acknowledgements This research is partly supported by the National Natural Science Foundation of China (61773064, 61503028), Graduate Technological Innovation Project of Beijing Institute of Technology (2018CX10022) and National High Tech. Research and Development Program of China (No. 2015AA043202).

Author contributions Huiming Xing designed and modeled the composite driving mechanism, conducted the experiments and drafted this paper. Shuxiang Guo has contributed significantly to data analysis, manuscript preparation, and revising it critically for important intellectual detail. Liwei Shi has contributed to the conception of the study and helped perform the analysis with constructive discussions. Xihuan Hou, Yu Liu, Huikang Liu helped to do these experiments.

References

Bak J, Nguyen HN, Park S, Lee D, Seo TW, Jin S, Kim J (2017) Positioning control of an underwater robot with tilting thrusters via decomposition of thrust vector. Int J Control Autom Syst 15(5):1–9

Crespi A, Ijspeert AJ (2008) Online optimization of swimming and crawling in an amphibious snake robot. IEEE Trans Robot 24(1):75–87

Crespi A, Karakasiliotis K, Guignard A, Ijspeert AJ (2013) Salamandra robotica II: an amphibious robot to study salamander-like swimming and walking gaits. IEEE Trans Robot 29(2):308–320

Gu S, Guo S (2017) Performance evaluation of a novel propulsion system for the spherical underwater robot (SURIII). Appl Sci 7(11):1197

Guo X, Ma S, Li B, Fang Y (2018a) A novel serpentine gait generation method for snake-like robots based on geometry mechanics. IEEE ASME Trans Mechatron 23(3):1249–1258

Guo S, He Y, Shi L, Pan S, Xiao R, Tang K, Guo P (2018b) Modeling and experimental evaluation of an improved amphibious robot with compact structure. Robot Comput Integr Manuf 51:37–52

Hou X, Guo S, Shi L, Xing H, Liu Y, Liu H, Hu Y, Xia D, Li Z (2019) Hydrodynamic analysis-based modeling and experimental verification of a new water-jet thruster for an amphibious spherical robot. Sensors 19:259

Jia L, Hu Z, Geng L, Yang Y, Wang C (2016) The concept design of a mobile amphibious spherical robot for underwater operation. In: IEEE international conference on cyber technology in automation, control, and intelligent systems (CYBER). https://doi.org/10.1109/CYBER.2016.7574860

Jin S, Kim J, Kim J, Seo T (2015) Six-degree-of-freedom hovering control of an underwater robotic platform with four tilting thrusters via selective switching control. IEEE ASME Trans Mechatron 20(5):2370–2378

Kim HG, Lee DG, Jeong KM, Seo TW (2016a) Water and ground-running robotic platform by repeated motion of six spherical footpads. IEEE ASME Trans Mechatron 21(1):175–183

Kim H, Lee D, Liu Y, Jeong K, Seo T (2016b) Hexapedal robotic platform for amphibious locomotion on ground and water surface. J Bionic Eng 13(1):39–47

Li M, Guo S, Hirata H, Ishihara H (2015) Design and performance evaluation of an amphibious spherical robot. Robot Auton Syst 64:21–34

Li M, Guo S, Hirata H, Ishihara H (2017) A roller-skating/walking mode-based amphibious robot. Robot Comput Integr Manuf 44:17–29

Lin X, Guo S, Yue C, Du J (2013) 3D modelling of a vectored water jet-based multi-propeller propulsion system for a spherical underwater robot. Int J Adv Robot Syst 10(1):1–8

Shen Y, Pu H, Sun Y, Ma S, Xie S, Luo J, Jia W (2016) Generating vectored thrust with the rotational paddling gait of an ePaddle-EGM mechanism: modeling and experimental verifications. IEEE J Ocean Eng 42(3):522–531

Shen Y, Sun Y, Pu H, Ma S (2017) Experimental verification of the oscillating paddling gait for an ePaddle-EGM amphibious locomotion mechanism. IEEE Robot Autom Lett 2(4):2322–2327

Shi Q, Ishii H, Kinoshita S, Konno S, Takanishi A, Okabayashi S, Iida N, Kimura H, Shibata S (2013) Modulation of rat behaviour by using a rat-like robot. Bioinspir Biomim 8(4):046002

Shi Q, Ishii H, Sugahara Y, Sugita H, Takanishi A, Huang Q, Fukuda T (2015a) Design and control of a biomimetic robotic rat for interaction with laboratory rats. IEEE ASME Trans Mechatron 20(4):1832–1842

Shi Q, Ishii H, Tanaka K, Sugahara Y, Takanishi A, Okabayashi S, Huang Q, Fukuda T (2015b) Behavior modulation of rats to a robotic rat in multi-rat interaction. Bioinspir Biomim 10(5):050611

Xing H, Guo S, Shi L, He Y, Su S, Chen Z, Hou X (2018a) Hybrid locomotion evaluation for a novel amphibious spherical robot. Appl Sci 8(2):156

Xing H, Guo S, Shi L, Hou X, Su S, Chen Z, Liu Y, Liu H (2018b) Performance evaluation of a multi-vectored water-jet propellers device for an amphibious spherical robot. In: IEEE International conference on mechatronics and automation. https://ieeexplore.ieee.org/document/8484441

Xing H, Shi L, Tang K, Guo S, Hou X, Liu Y, Liu H, Hu Y (2019) Robust RGB-D camera and IMU fusion-based cooperative and relative close-range localization for multiple turtle-inspired amphibious spherical robots. J Bionic Eng 16(3):442–454

Yang Y, Zhou G, Zhang J, Cheng S, Fu M (2015) Design, modeling and control of a novel amphibious robot with dual-swing-legs propulsion mechanism. In: IEEE/RSJ international conference on intelligent robots and system (IROS). https://ieeexplore.ieee.org/document/7353427

Yu J, Ding R, Yang Q, Tan M, Wang W, Zhang J (2012) On a bio-inspired amphibious robot capable of multimodal motion. IEEE ASME Trans Mechatron 17(5):847–856

Yu J, Ding R, Yang Q, Tan M, Zhang J (2013) Amphibious pattern design of a robotic fish with wheel-propeller-fin mechanisms. J Field Robot 30(5):702–716

Zhang S, Zhou Y, Xu M, Liang X, Liu J, Yang J (2016) AmphiHex-I: locomotory performance in amphibious environments with specially designed transformable flipper legs. IEEE ASME Trans Mechatron 21(3):1720–1731

Zheng L, Guo S, Gu S (2018) The communication and stability evaluation of amphibious spherical robots. Microsyst Technol 24:1–12

Zhong B, Zhang S, Xu M, Zhou Y, Fang T, Li W (2018) On a CPG-based hexapod robot: AmphiHex-II with variable stiffness legs. IEEE ASME Trans Mechatron 23(2):542–551